UNIVERSITY OF THESSALY
SCHOOL OF ENGINEERING
DEPARTMENT OF MECHANICAL ENGINEERING

FATIGUE AND FATIGUE CRACK PROPAGATION OF (Al-Cu-Li) AA2198 FOLLOWING ARTIFICIAL AGING

by

IOANNIS GOULAS
Mechanical Engineer, University of Thessaly, 2022

Submitted in partial fulfillment of the requirements for the degree of Master of Science in Mechanical Engineering at the University of Thessaly

Volos, 2024

UNIVERSITY OF THESSALY
SCHOOL OF ENGINEERING
DEPARTMENT OF MECHANICAL ENGINEERING

FATIGUE AND FATIGUE CRACK PROPAGATION OF (Al-Cu-Li) AA2198 FOLLOWING ARTIFICIAL AGING

by

IOANNIS GOULAS

Submitted in partial fulfillment of the requirements for the of Master of Science in Mechanical Engineering at the University of Thessaly

Volos, 2024

Approved by the Committee on Final Examination:

Advisor	Dr. Alexis Kermanidis, Associate Professor, Department of Mechanical Engineering, University of Thessaly
Member	Dr. Gregory Haidemenopoulos, Professor, Department of Mechanical Engineering, University of Thessaly
Member	Dr. Emmanouil Bouzakis, Associate Professor, Department of Mechanical Engineering, University of Thessaly

Date Approved: [February 29, 2024]

Acknowledgements

First, I would like to express my sincere thanks to my thesis supervisor, Associate Professor Alexis Kermanidis, for his valuable help and guidance during my MSc studies, and for our collaboration in the Laboratory of Mechanics & Strength of Materials of the University of Thessaly.

I am also grateful to the other members of the examination committee of my master thesis, Professor Gregory Haidemenopoulos and Associate Professor Emmanouil Bouzakis for their careful reading of my thesis and for their valuable suggestions.

A part of this research was carried out within the framework of the program "CorLi" (Corrosion susceptibility, degradation and protection of Al-Li aluminum alloys). I would like to especially thank the program partners Associate Professor Nikolaos Alexopoulos, and Dr. Christina Margarita Charalampidou for their important support.

I am also thankful to Dr. Theocharis Papatheocharis, PhD Candidate Aris Stamou and my colleague and friend George Vomvyras-Vartis for their help, support and encouragement throughout my studies.

Finally, but above all, I am grateful to my parents Thanasis and Stavroula and my sister Christina for their wholehearted love and support all these years, contributing not only morally but also financially to my studies.

FATIGUE AND FATIGUE CRACK PROPAGATION OF (Al-Cu-Li) AA2198 FOLLOWING ARTIFICIAL AGING

IOANNIS GOULAS

Department of Mechanical Engineering, University of Thessaly

Supervisor: Dr Alexis Kermanidis

Associate Professor

Abstract

Third generation Al-Cu-Li alloys are attractive alternatives to the conventional alloys from the 2xxx series (e.g. AA2024) and are utilized in aircraft fuselage skin applications due to their exceptional mechanical properties, and improved fracture and corrosion resistance. Still, there is room for improvement of their fatigue and damage tolerance performance by careful manipulation of the concentration of alloying elements and heat treatment processing in order to control the development of strengthening precipitates.

In order to investigate the capacity of the (Al-Cu-Li) AA2198-T3 alloy to improve its fatigue and fatigue crack growth behavior, exposure of the alloy to various artificial aging conditions has been performed. The specific study aims also to provide valuable insight in terms of simulating the natural aging process that occurs during the long-term operation of the material. Based on the original T3 temper, four (4) distinct aging conditions were taken into consideration, corresponding to under-aged (UA), peak-aged (PA), and over-aged (OA) tempers. Constant amplitude high cycle fatigue and fatigue crack propagation tests have been conducted to evaluate the materials cyclic and fracture performance under artificial aging.

The high cycle fatigue results have shown that the reference material (T3) exhibits good fatigue performance compared to the other tempers. While in the reference T3 temper the material exhibits improved fatigue crack propagation (FCP) specifically at low ΔK levels, in the UA condition and medium to high ΔK values a more damage tolerant behavior is obtained.

Key words: *aluminum-lithium alloy, artificial ageing, constant amplitude fatigue, fatigue crack growth*

ΜΕΛΕΤΗ ΤΗΣ ΚΟΠΩΣΗΣ ΚΑΙ ΔΙΑΔΟΣΗΣ ΡΩΓΜΗΣ ΛΟΓΩ ΚΟΠΩΣΗΣ ΤΟΥ (Al-Cu-Li) AA2198 ΓΙΑ ΔΙΑΦΟΡΕΤΙΚΕΣ ΚΑΤΑΣΤΑΣΕΙΣ ΤΕΧΝΗΤΗΣ ΓΗΡΑΝΣΗΣ

ΙΩΑΝΝΗΣ ΓΟΥΛΑΣ

Τμήμα Μηχανολόγων Μηχανικών, Πανεπιστήμιο Θεσσαλίας, 2024

Επιβλέπων Καθηγητής: Δρ. Αλέξης Κερμανίδης,

Αναπληρωτής Καθηγητής

Περίληψη

Τα κράματα Al-Cu-Li τρίτης γενιάς αποτελούν ελκυστικές εναλλακτικές των συμβατικών κραμάτων της σειράς 2xxx (π.χ. AA2024) και χρησιμοποιούνται σε εφαρμογές όπως οι άτρακτοι αεροσκαφών λόγω των εξαιρετικών μηχανικών τους ιδιοτήτων και της βελτιωμένης αντοχής σε θραύση και διάβρωση. Ωστόσο, υπάρχει περιθώριο βελτίωσης της απόδοσης αντοχής σε κόπωση και θραύση με τον προσεκτικό χειρισμό της συγκέντρωσης των κραματικών στοιχείων και της θερμικής κατεργασίας προκειμένου να ελεγχθεί η ανάπτυξη σωματιδίων ενίσχυσης.

Προκειμένου να διερευνηθεί η ικανότητα του κράματος (Al-Cu-Li) AA2198-T3 να βελτιώσει τη συμπεριφορά του σε κόπωση και σε ανάπτυξη ρωγμών λόγω κόπωσης, πραγματοποιήθηκε έκθεση του κράματος σε διάφορες καταστάσεις τεχνητής γήρανσης. Η συγκεκριμένη μελέτη στοχεύει επίσης να προσφέρει πολύτιμες πληροφορίες όσον αφορά την προσομοίωση της φυσικής διαδικασίας γήρανσης που συμβαίνει κατά τη μακροχρόνια λειτουργία του υλικού. Με βάση την αρχική κατάσταση αναφοράς T3, λήφθηκαν υπόψη τέσσερις (4) διακριτές συνθήκες γήρανσης, που αντιστοιχούν σε υπό-γήρανση (UA), μέγιστη γήρανση (PA) και υπέρ-γήρανση (OA). Δοκιμές πολυκυκλικής κόπωσης σταθερού πλάτους τάσης και διάδοσης ρωγμών κόπωσης διεξήχθησαν για την αξιολόγηση της απόδοσης σε εναλλασσόμενη φόρτιση και της ανοχής σε βλάβη των υλικών υπό τεχνητή γήρανση.

Τα αποτελέσματα της πολυκυκλικής κόπωσης έδειξαν ότι το υλικό αναφοράς (T3) παρουσιάζει καλή απόδοση κόπωσης σε σύγκριση με τα δοκίμια τεχνητής γήρανσης. Ενώ το T3 υλικό εμφανίζει βελτιωμένη απόδοση σε διάδοση ρωγμών κόπωσης, ειδικά σε χαμηλά εύρη ΔK, στην κατάσταση UA και σε μεσαίες έως υψηλές τιμές ΔΚ παρατηρείται μια πιο ανθεκτική στη βλάβη συμπεριφορά.

***Λέξεις-κλειδιά**: κράμα αλουμινίου-λιθίου, τεχνητή γήρανση, κόπωση σταθερού πλάτους, εξέλιξη ρωγμής σε κόπωση*

Table of Contents

List of tables

List of figures

Abbreviations

Al	Aluminum
AA	Aluminum association
COD	Crack opening displacement
C(T)	Compact tension
Cu	Copper
DSLR	Digital single-lens reflex
FCG	Fatigue Crack Growth
FCGR	Fatigue Crack Growth Rate
FCP	Fatigue Crack Propagation
Fe	Ferrum
GPa	Gigapascal
h	hours
HCF	High cycle fatigue
kN	kiloNewton
LEFM	Lineal Elastic Fracture Mechanics
Li	Lithium
LCF	Low cycle fatigue
Mg	Magnesium
MPa	Megapascal
Mn	Manganese
OA	Over-ageing
PA	Peak-ageing
Si	Silicon

UA	Under-ageing
Zn	Zinc
Zr	Zirconium

Symbols

a	crack length
α	crack length to width ratio
b	basquin exponent
C	parameter of Paris equation
C_0	equivelant parameter of Paris equation stress ratio equal to zero
da/dN	fatigue crack growth rate
E	Young's modulus
F	frequency
K_{cr}	critical stress intensity factor
K_{max}	maximum value of the stress intensity factor
K_{min}	minimum value of the stress intensity factor
m	Paris equation exponent
R	stress ratio
N_f	fatigue life
Δa	crack growth increment
ΔK	stress intensity factor range
ΔK_{th}	stress intensity threshold
σ_a	stress amplitude
$\sigma_{a,eq}$	equivalent stress amplitude for zero mean stress
$\sigma_{f'}$	cyclic stress basquin coefficient
σ_m	mean stress
σ_{max}	maximum stress value

σ_{min}	minimum stress value
σ_{uts}	ultimate tensile strength
σ_{y}	yield stress
$\sigma_{y,0.2\%}$	conventional 0.2% yield stress

Chapter 1: Introduction

1.1 Description of the technological problem – Motivation

Aluminum-lithium (Al-Li) alloys have drawn a lot of interest during the last decades from the aerospace industry because they combine low density with enhanced mechanical performance and damage tolerance (fatigue crack propagation and fracture toughness) [1], [2], [3]. The aforementioned benefits are contingent upon the existence of Li and the intricate precipitation hardening mechanism, which encompasses many strengthening intermetallic phases, including δ (Al_3Li), T_1 (Al_2CuLi), ϑ (Al_2Cu) and S (Al_2CuMg) [4].

Comparing the most recent generation of 2xxx series Al-Li alloys to the traditional 2024 aluminium alloy, incremental microstructural advances over the previous generations have resulted in a systematic improvement in the alloys' fatigue and damage tolerance characteristics. In a comparison study, Alexopoulos et al. [2] shown that the fatigue endurance limit of AA2024-T3 is around 40% below its yield stress, but it is just 9% below for AA2198-T351, with the two alloys exhibiting comparable levels of fatigue limit values. It was claimed in [5] that low levels of plastic pre-deformation combined with regulated mechanical processing might increase fatigue resistance even further.

Damage tolerance under cyclic loading has been a strong attribute of the second-generation Al-Li alloys. It was demonstrated in [6] that the very tortuous fatigue profile of AA 2090 thick plates, which results in high crack closure levels, was the cause of the low fatigue crack propagation rates of those plates. The fatigue crack propagation properties have been significantly improved in more modern Al-Li alloy systems. Even though some anisotropy was noted, the AA2198-T851 alloy in the investigation by [7] typically had a more competent fatigue crack propagation behaviour than the AA2024-T3 alloy.

Depending on the alloy and temper, hardening precipitates have a considerable effect on the pace at which fatigue cracks form. Lower fatigue life and cyclic softening phenomena were seen when artificial ageing of Al-Li alloys was increased. This was because the interactions between microstructural characteristics, such as precipitations, led to greater development and growth of cracks [8]. Although there are reports available, systematic investigations on the role of ageing on fatigue and damage tolerance behaviour of new generation Al-Li are still lacking. This is in the context of exploring appropriate processing routes for the development of light alloys with superior damage tolerance characteristics, but also examine the effect of long-term natural aging on material performance.

1.2 Modern applications of Al-Li alloys

Aircraft structure applications such as fuselage skins, floor beams, and floor support structures are the primary applications for Al-Li alloys [9]. The passenger airplane C919 (**Fig. 1**) has several structural components made of Al-Li alloys. New technology and manufacturing methods have been quietly revolutionizing the aviation business, particularly with the next generation of commercial twin-aisle aircraft, which includes the Airbus A350 (fuselage skin **Fig. 2**) and Boeing 787 Dreamliner. The Boeing 777-9 features an aluminum-primarily fuselage (**Fig. 3**) with composite wings. This shift is the result of the development of sophisticated third-generation aluminum-lithium (Al-Li) alloys, which are stronger and lighter than earlier versions while also being less expensive than both carbon fiber-reinforced plastic (CFRP) and titanium alloys. Consequently, airplanes with a high Al-Li alloy content use less fuel and require less maintenance [10]

(a)

(b)

Fig. 1: (a) Model of the C919 from China Eastern Airlines, (b) fuselage skin of C919 [11], [12]

Fig. 2: Fuselage skin of Airbus A350 [13]

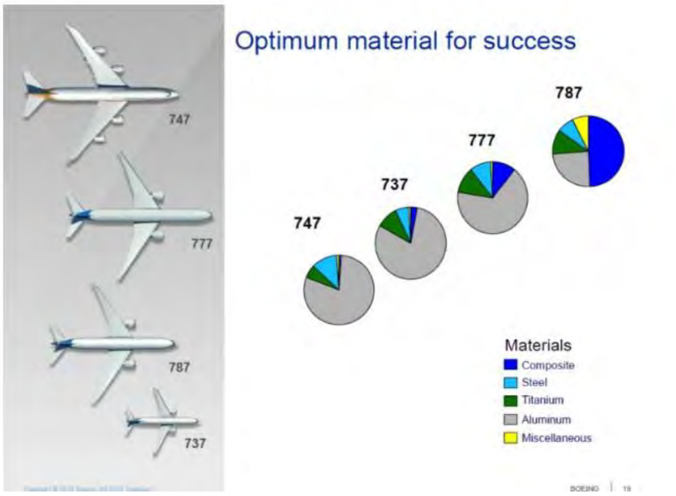

Fig. 3: Distribution of materials in different Boeing models [10]

Aluminium lithium alloys also used in the SpaceX Falcon 9 spacecraft's fuselage components and second-stage fuel tanks (**Fig. 4**). The walls and domes of the propellant tank are composed of Al-Li alloys. SpaceX uses a tank that is fully friction-stir welded because of its durability and dependability. The second stage tank is a condensed version of the first stage tank [14].

Fig. 4: Depiction of SpaceX Falcon 9 [14]

Al-Li alloys are appropriate for use in rivets, structural airplanes, as well as space applications, including rocket structures like fuel tanks and canopies. (**Fig. 5**). NASA claims that by substituting an Al-Cu-Li alloy for older metals in the structure of its fuel tanks, the structure's weight was lowered by three tons, earning it the name Super Lightweight Tank (SLWT) [15].

Fig. 5: Tank construction by NASA using Al-Li alloy, SLWT [15]

1.3 Master thesis organization

The master thesis is developed in six (6) Chapters. In **Chapter 2** the basic points of fatigue theory are analyzed. Among other things, the two basic fatigue design philosophies are addressed, as well as key elements of linear elastic theory that are essential for fatigue damage tolerance design. **Chapter 3** focuses on fatigue of aluminum-lithium alloys and in particular the AA2198 and some key points of aging heat treatment are analyzed. In **Chapter 4** the tests and the material used as well as the two (2) experimental procedures are described. In **Chapter 5** the experimental results of the tensile tests, constant amplitude fatigue and fatigue crack growth tests are presented and discussed. **Chapter 6** provides an overview of the investigation's key conclusions as well as recommendations for further research in this area.

Chapter 2: Fatigue design philosophies

2.1 Design based on S-N behavior

In the fatigue test, a specimen is subjected to a variable load while keeping the mean stress (σ_m) and stress amplitude (σ_a) constant and the number of loading cycles N_f below which the material fails (fracture) is determined. To plot the S-N curves, an experimental series is created in which the mean stress is kept constant while the stress amplitude is varied each time. It should be noted that the results are represented in a log-log scale diagram [16].

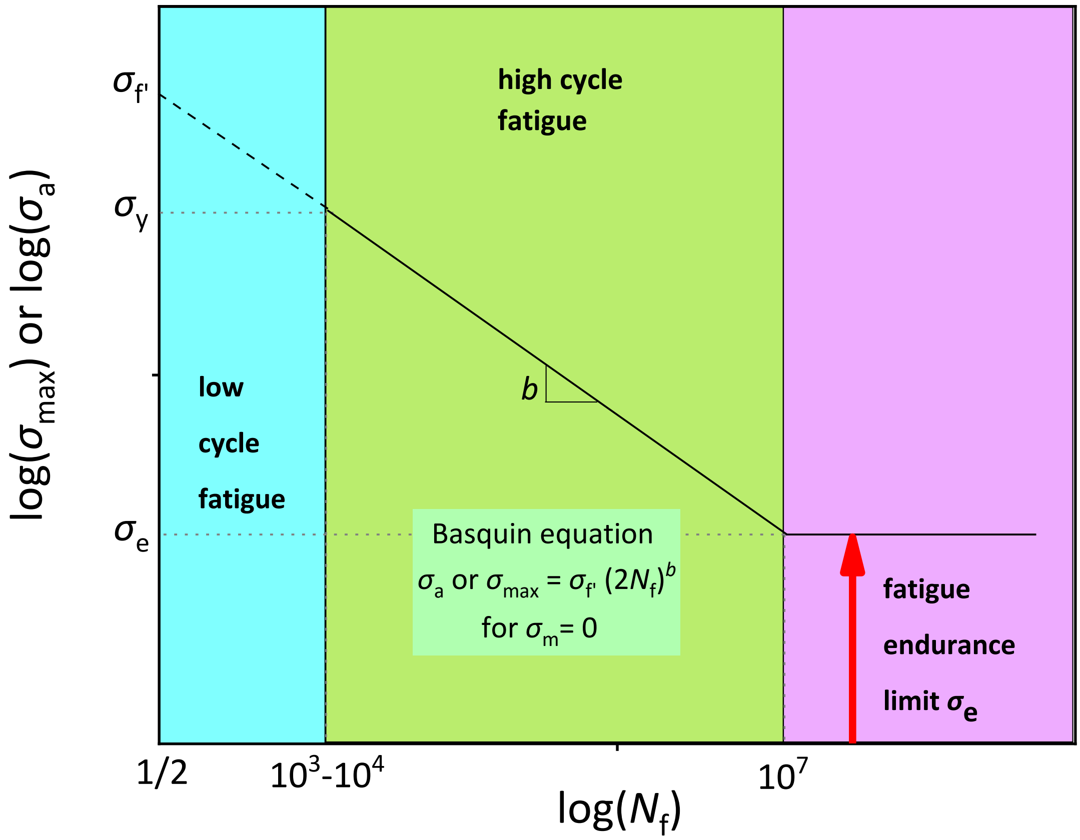

Fig. 6: Characteristic S-N curve

Fig. 6 shows the following three areas:

- The low cycle fatigue region is characterized by high stress amplitudes and the number of cycles leading to failure is up to 10^3-10^4 fatigue cycles. In this region the material undergoes elastoplastic deformation.
- The high cycle fatigue region where stress amplitudes lead to failure cycles between 10^3-10^4 to 10^7 load cycles.

- The region of fatigue endurance limit where the specimen does not fail no matter how large the number of loading cycles N is below a certain stress amplitude which is called fatigue endurance limit. Note that fatigue life design requires the amplitude of the applied stresses to be below the fatigue limit of the material.

2.2 Design based on damage tolerance

The existence of a crack has significant effect on the mechanical behavior of a mechanical component as it causes a local stress concentration. This indicates that compared to the rest of the material, the stresses in the region of the fracture are substantially greater. Consequently, the material's behavior is deteriorated under fatigue, thus lowering its lifespan. Furthermore, it can be costly to fix cracks, and oftentimes the element cannot be fully restored. Cracks frequently have the power to destroy the structure, putting human lives and the environment at danger. Taking these into account, the urgent need to study the effect of cracks on a mechanical element becomes immediately apparent.

Fatigue crack propagation can be plotted as a plot of crack growth rate da/dN versus the range of the stress intensity factor ΔK on a log-log scale. The ΔK range is defined by the equation:

$$\boldsymbol{\Delta K = Y * \Delta\sigma * \sqrt{\pi * \mathrm{a}}} \qquad (1)$$

where $\Delta\sigma$ is the stress range, Y is a correction factor that depends on the geometry and a is the crack length.

Note that the diagram is a property of the material and can thus be used during design. Also, damage tolerance design requires frequent monitoring by the engineer and for this reason inspection intervals are specified [17].

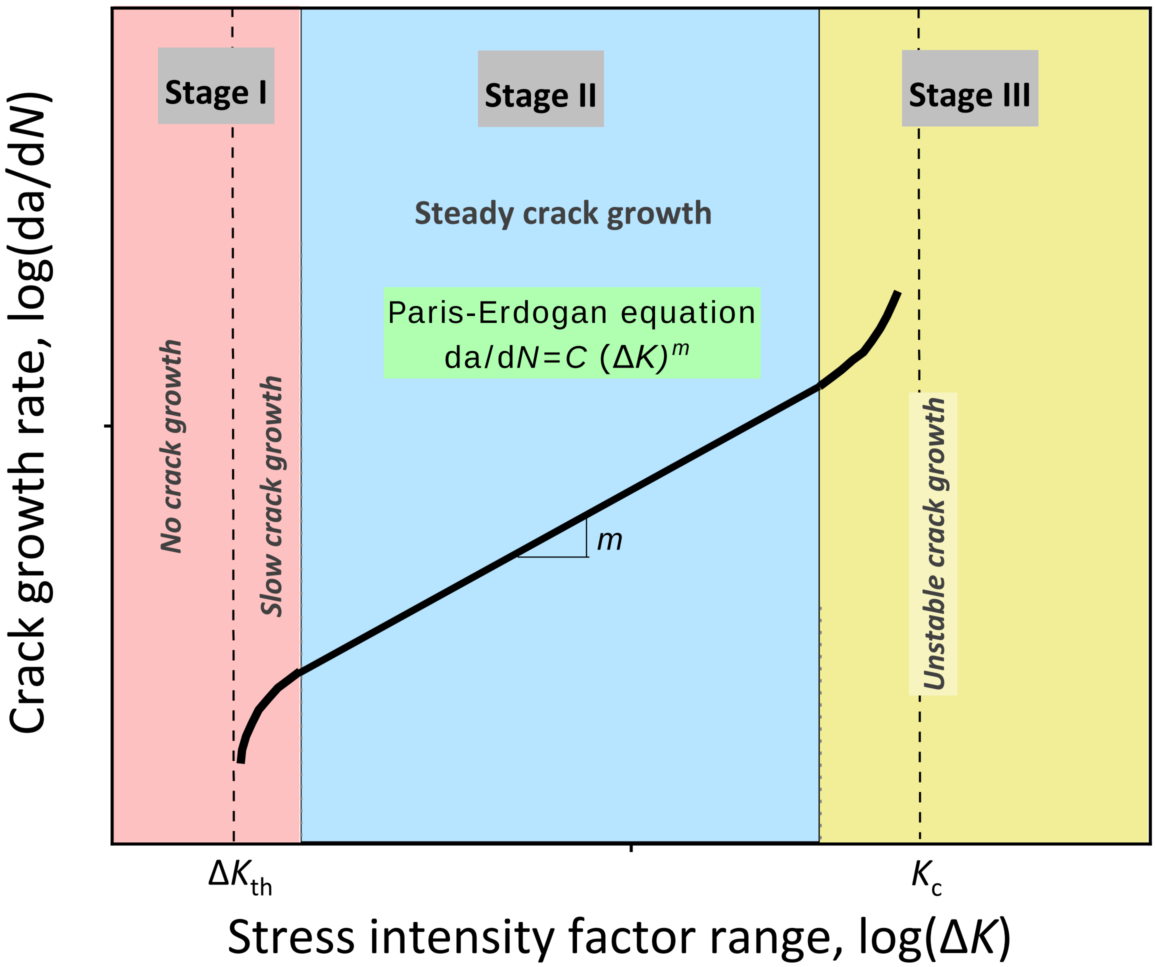

Fig. 7: Characteristic da/d*N* – Δ*K* curve

The diagram in **Fig. 7** shows the following three areas:

- Stage I represents the first stage of crack growth and microcrack propagation. The crack growth rate is typically of the order of 10^{-6} mm/cycle or even smaller. This area is considered quite sensitive and is mainly influenced by the microstructure of the material, the mean stress and the temperature. Here there is a threshold range ΔK_{th} where for values smaller than this, no crack propagation is observed. It is worth mentioning that the ΔK_{th} value is used as a design parameter.
- Stage II (Paris-Erdogan equation) represents an intermediate stage of crack propagation, where the size of the plastic zone created is now comparable with the average grain size of the material. The usage of the basic principles of the Linear Elastic theory of fracture mechanics in this point is acceptable and the points between da/dN and ΔK present linearity in log-log scale. The crack propagation rate is now on the order of 10^{-6}-10^{-3} mm/cycle.

- Stage III represents the fastest crack length growth, with high rates (>10^{-3}mm/cycle) due to the fast and unstable propagation of cracking before fracture. The relationship between da/d*N* and Δ*K* is nearly exponential, and *K*'s value is getting closer to the material's critical fracture toughness value, K_c. Stress levels are rather high in front of the crack, which encourages the development of a huge plastic zone. The theory of Linear Elastic Fracture Mechanics leads to erroneous considerations at this point and because of the quick yielding at material, and Plastic Elasticity is the theory that can explain the phenomena.

2.3 Plasticity limitations on LEFM

The equations that estimate the size of plastic zones under plane stress is:

$$\sigma_x = \sigma_{\upsilon} = \frac{K}{\sqrt{2\pi r}},\ \ \sigma_z = \tau_{x\upsilon} = \tau_{yz} = \tau_{xz} = 0 \qquad (2)$$

The distance r_y where the elastic stress distribution surpasses the yield requirement for plane stress prior to the crack tip is estimated when the stresses $\sigma_x = \sigma_\upsilon$ are equal to yield stress σ_y.

$$\boldsymbol{r_y = \frac{1}{2\pi}\left(\frac{K}{\sigma_y}\right)^2} \qquad (3)$$

It is possible to determine the coefficient K with high precision as long as the fracture is located in a homogenous intense field. This strategy is particularly challenging, though, in complicated, intense domains [18].

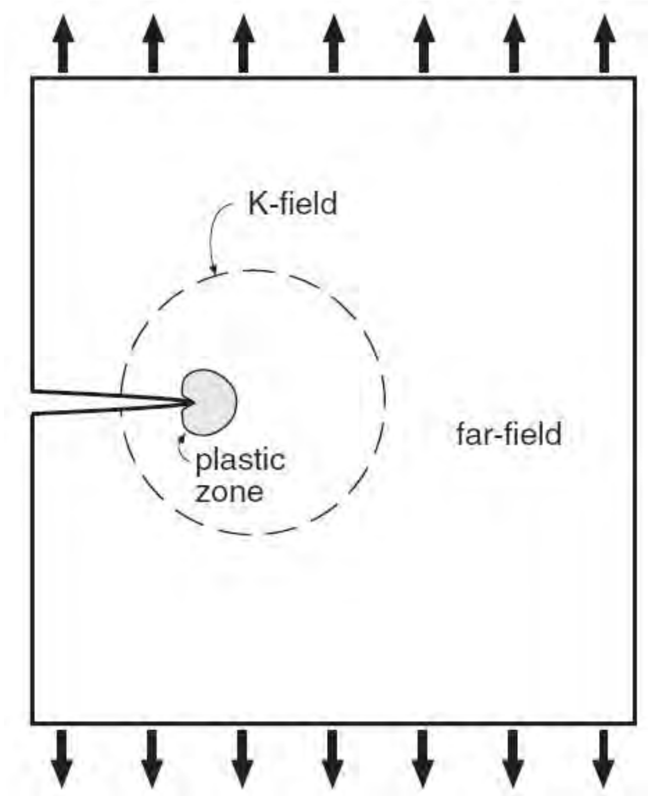

Fig. 8: A crack and the plastic zone surrounding it, as well as the greater K-field required for LEFM to be relevant [18]**.**

Linear Elastic Fracture Mechanics (LEFM) Theory concepts can be applied when the plastic zone is contained to a limited area surrounding the tip fracture and the field K is substantially bigger than the plastic region (**Fig. 8**). Otherwise, the Linear Elastic Theory will produce errors and the Elastic-Plastic Theory must be applied when the plastic zone is significantly greater than the crack length or the remaining cross-section.

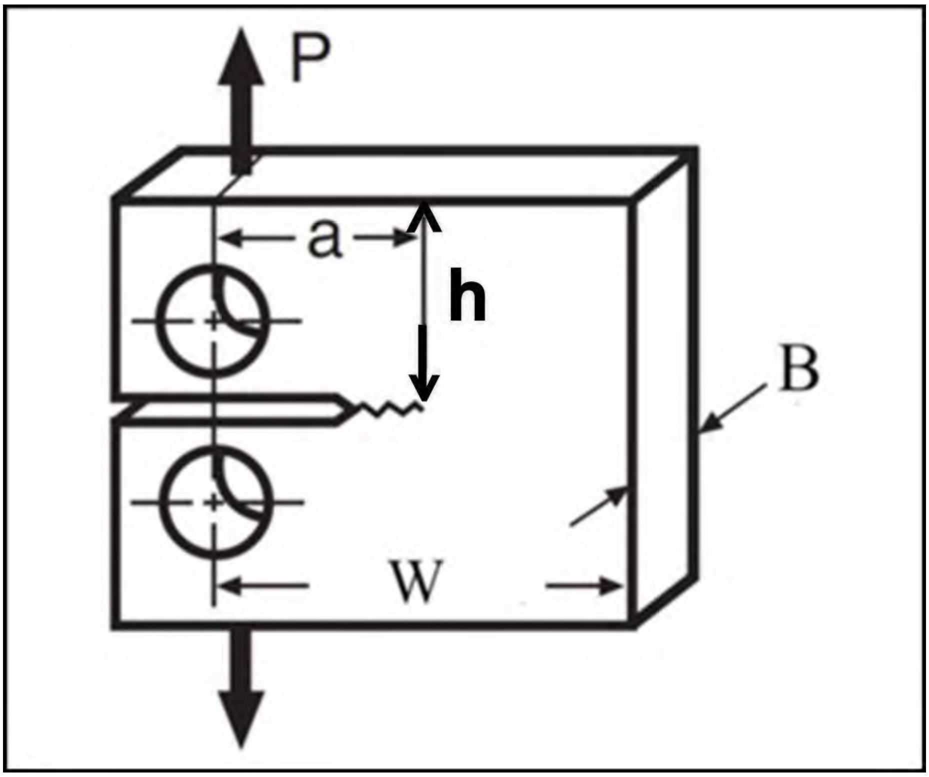

Fig. 9: Prototype specimen with side crack

In more detail, a generic limit that links the geometric characteristics of the specimens and the crack with the stress intensity factor K has been presented for the application of the principles guiding linear elasticity theory. Based in **Fig. 9** this limit is determined by:

$$\mathbf{a}, (\boldsymbol{W} - \mathbf{a}), \boldsymbol{h} \geq \frac{4}{\pi}\left(\frac{K}{\sigma_y}\right)^2 \qquad (4)$$

, where W is the width, σ_y is the yield strength of the material, (W-a) is the uncracked area of the specimen and h is the vertical distance of the crack plane from the free surface. The inequality described by Eq. 2 must be satisfied for all three dimensions a, W-a, h. Otherwise, the intense situation that prevails near the peak of the crack causes intense plasticity phenomena and the plastic zone exceeds in size the K field [18].

Chapter 3: Literature review

3.1 Categorization of aluminum alloys

Aluminum alloys are separated into two (2) types: wrought alloys, which are formed by working the metal into a certain shape, and cast alloys, which are poured into a mold that takes on a specific shape while still molten. The interest is focused on the wrought alloys, which in the Aluminum Association's designation system, any alloy that is registered with the association is given a four-digit (4) number. An alloy's major alloying element is indicated by its first number, which results in an alloy family with related qualities. By association, the final two numbers are allocated in a consecutive order. An alloy alteration is indicated by the second number. One extra sign that often appears after the four-digit number indicates the treatments the alloy has received. The first letter T (Thermal) followed by a number indicates that it has undergone thermal treatment. In **Table 1** are summarized the primary alloying elements and the properties of the resulting alloys [19].

Table 1: Wrought alloy designation system and characteristics [19]

Series Number	Primary alloying element	Relative Strength	Heat Treatment
1XXX	None	Fair	Non-heat-treatable
2XXX	**Copper**	**Excellent**	**Heat treatable**
3XXX	Manganese	Fair	Non-heat-treatable
4XXX	Silicon	-	Non-heat-treatable
5XXX	Magnesium	Good	Non-heat-treatable
6XXX	Magnesium and Silicon	Good	Heat treatable
7XXX	Zinc	Excellent	Heat treatable

3.1.1 Aluminum alloy 2198

Compared to commercially available 2xxx series Al alloys, third generation Al-Cu-Li alloys are very advantageous materials with increased tensile mechanical characteristics and enhanced damage tolerance. AA2198 is an alloy that exhibits exceptional structural efficiency because of its high strength and low density. **Table 2** displays Al-Li alloy 2198's chemical composition.

Table 2: Chemical composition of aluminum alloy 2198 (percentages in % by weight)

Alloy	Cu	Li	Zn	Mn	Mg	Zr	Si	Ag	Fe
2198	2.9-3.5	0.8-1.1	≤ 0.35	≤ 0.5	0.25-0.8	0.04-0.18	≤ 0.08	0.1-0.5	≤ 0.01

3.2 Fatigue of Al-Li alloys

Alexopoulos et al. in [2] among others they studied fatigue behavior of wrought AA2198-T351 in comparison with the AA2024. By carrying out constant amplitude fatigue tests, they concluded that the fatigue endurance limit is approximately 240 MPa. This value is only 9% below the yield stress (≈ 265 MPa) of the alloy, when the fatigue limit is 40% below the yield stress in the case of AA2024. In another study, Zhang et al. [5] explored the effect of pre-deformation of AA2198-T3 alloy. They found that for small amounts of plastic pre-deformation, the fatigue endurance limit decreased. Especially, when they enforced 3% and 5% pre-deformation at the material, they calculated that the fatigue endurance limit was 150MPa and 108MPa respectively. In addition, it is worth noting, that AA2198-T851 showed a lower fatigue limit than the AA2024 in both L and LT orientations for completely reversed cyclic and cycling under positive stress ratio, e.g. [7].

Regarding to damage tolerance behavior, Sepe et al. [7] discovered initially that AA2198-T851 in L orientation has slightly better FCP behavior than in LT orientation, fact that shows a certain anisotropy. Despite this the overall study showed that 2198-T851's mechanical performances were 5 to 30% better than 2024-T3's. According to the results of Jesus et al. [20] , the AA2050 in T8 temper showed reduced fatigue crack growth rates in comparison to the high strength 7050 T7451 alloy.

3.3 General principles of Al-Li alloys aging heat treatment

The precipitation of a second phase or an intermetallic phase from a supersaturated solid solution is one of the most important strengthening methods of aluminum alloys. The precipitate of the second phase in the form of a fine dispersion of particles, prevents the slip of dislocations and increases the strength of the alloy [21]. With the right thermal treatments, various precipitates can be produced. The particles of the new phase are called precipitates and the whole process is called precipitation hardening or age hardening. The various phases that are created exhibit varying resistances to keep dislocations from sliding. The strength of the material rises as a result of the fine particles that are created inside the grains, **Fig. 10**, which limit the passage of dislocations.

After the solid solution heat treatment, rapid cooling follows, which called quench and finally the alloy at room temperature reaches equilibrium. So, the T3 treatment is described in which we have the formation a of supersaturated solution. The supersaturated solid solution is heated to an intermediate temperature for the aging heat treatment in order to produce fine precipitates in the grains, as shown in **Fig. 11**. The usual aging behavior of a wrought alloy is as follows: the strength gradually increases over time, reaching a maximum value before finally declining. Peak aging refers to this strength growth up to the maximum value, whereas over aging refers to the long-term loss of hardness and strength.

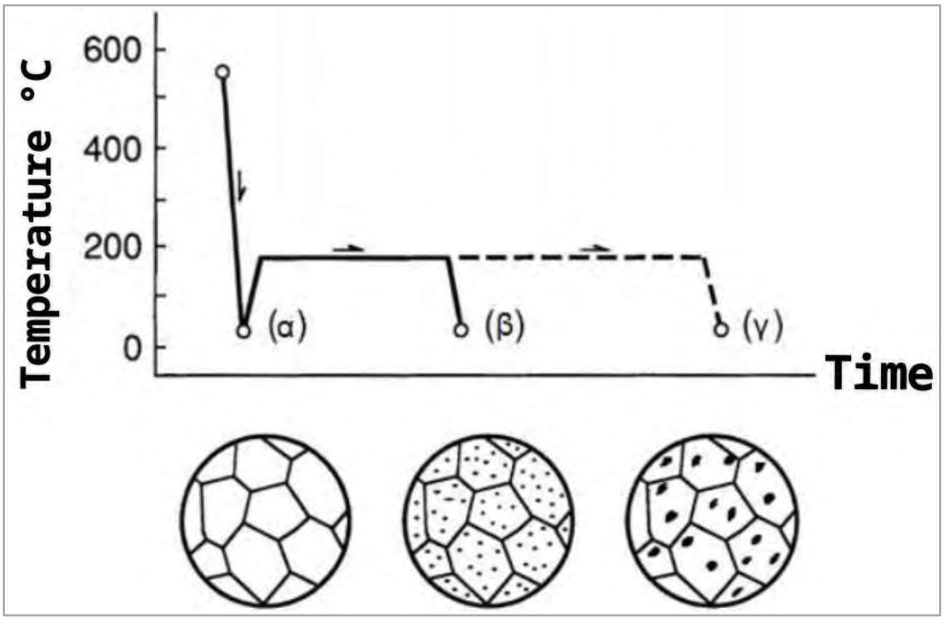

Fig. 10: Stages of artificial aging of aluminum alloy. (a) supersaturated solution after T3, under-aged, (b) aging at moderate temperature and obtaining fine precipitates in the grains, peak aged, (c) coarse precipitates, over aged.

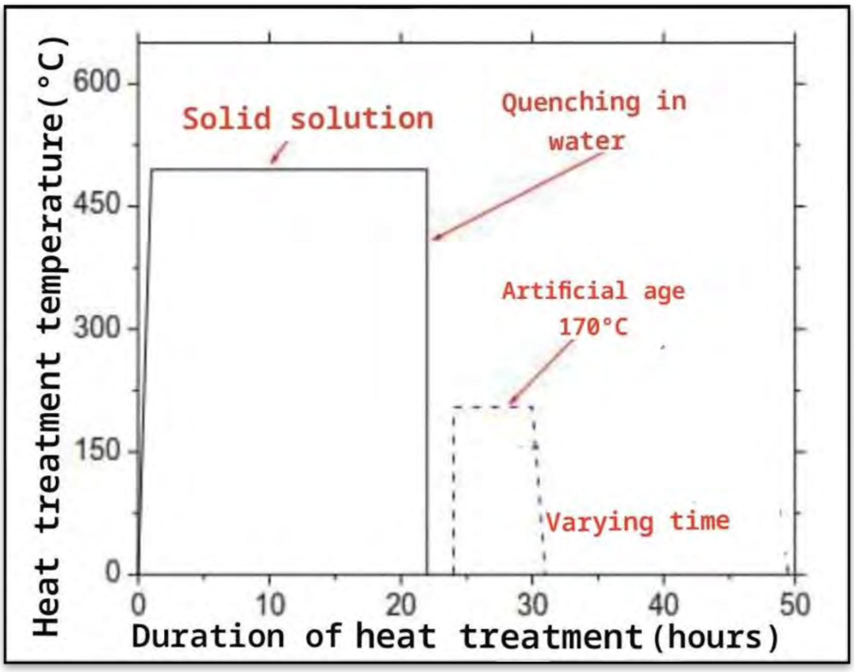

Fig. 11: Schematic representation of T3 treatment and artificial aging of aluminum alloy

Chapter 4: Experimental method

4.1 Materials and specimens

The current investigation employed samples from the commercially available wrought AA2198 alloy in T3 temper. According to the sheet manufacturer (Constellium), T3 temper comprises solution heat-treatment at 495 °C, quenching in water at 0 °C, and natural aging in room temperature (25 °C) to a basically stable condition. Al-Li alloy 2198's chemical composition is shown in **Table 2**.

To simulate the aging process of AA2198-T3, an isothermal artificial ageing heat-treatment was conducted at 170 °C in the condition that was received, which is T3. The heat treatment of the specimens was carried out by Alexopoulos et al. according to a previous publication [22]. The artificial ageing of AA2198-T3 (which ranges from 170 °C to 210 °C) was conducted at the lowest heat-treatment temperature of 170 °C because it is well-known that lower ageing temperatures allow for the well-balanced formation of coherent and subsequent, semi-coherent precipitates, respectively, leading to higher peak strengths [23]. Four (4) distinct artificial ageing durations were chosen for the current investigation, i.e., 3, 48, and 98 hours (also 400 hours for FCP tests), corresponding to the different examined situations, namely under-aged (UA), peak-aged (PA), and over-aged (OA). The specimens of AA2198-T3 were subjected to constant amplitude fatigue and fatigue crack growth tests after being artificially aged isothermally in an Elvem T101 (2600 W) electric oven of the Laboratory of Strength of materials, School of Applied Mathematical and Physical Sciences, National Technical University of Athens.

The fatigue and Compact Tension (hereafter referred to as C(T)) coupons were machined in accordance with ASTM E466 [24] and ASTM E647 [25] specifications, respectively, and from the longitudinal (L) rolling direction. The specimens' geometry and dimensions (in mm) are displayed in **Fig. 12**.

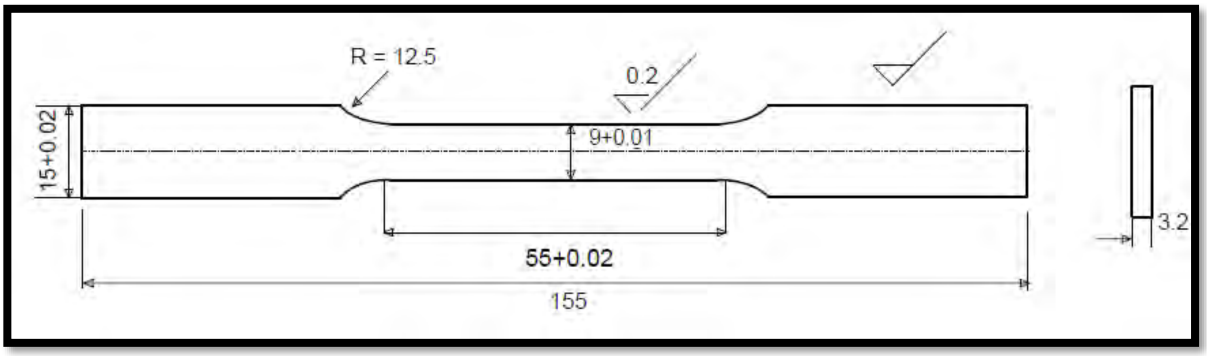

(a)

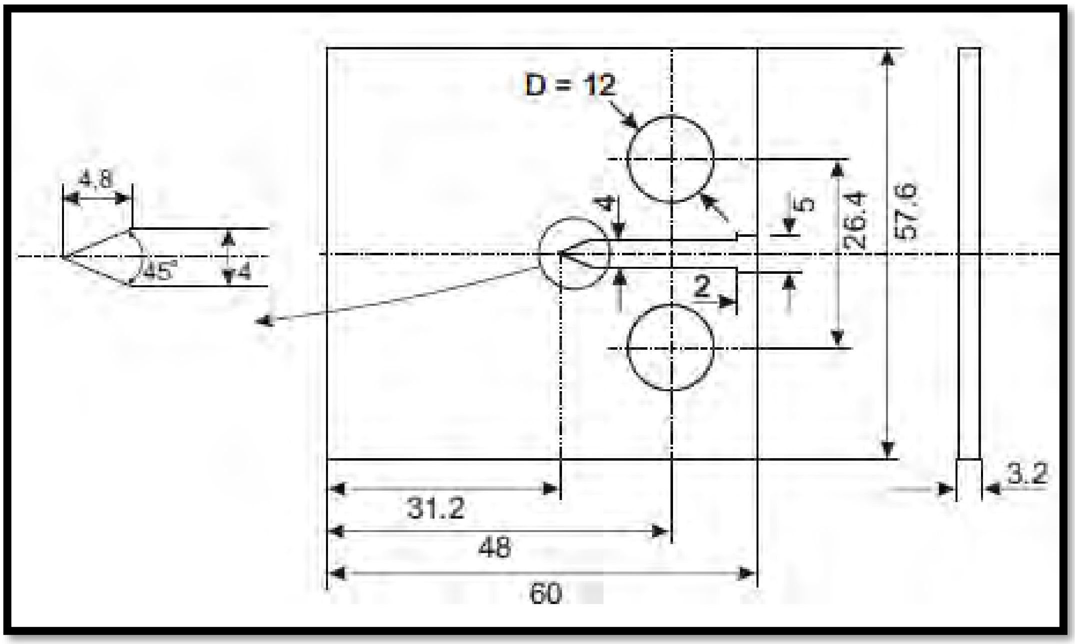

(b)

Fig. 12: Specimens geometry for (a) fatigue test and (b) fatigue crack growth (FCP) test.

4.2 Mechanical testing

The mechanical performance of AA2198 has been investigated through an experimental program that includes constant amplitude fatigue testing and fatigue crack growth (FCG). In **Table 3** a description of the performed experimental program is presented.

Table 3: Description of experimental program.

No	Material	Treatment	Constant amplitude fatigue tests [-]	Fatigue crack propagation tests [-]
1	**AA2198-T3**	No treatment (tested at the initial T3 temper)	13	4
2	**AA2198-UA**	Under-aged - UA (T3 + 3 h @ 170 °C)	14	3
3	**AA2198-PA**	Peak aged - PA (T3 + 48 h @ 170 °C)	19	3
4	**AA2198-OA**	Over aged - OA (T3 + 98 h @ 170 °C)	14	3

4.2.1 Constant amplitude fatigue tests

A uniaxial, servo-hydraulic, Instron 8801 machine with a 100 kN load cell was used to conduct constant amplitude fatigue testing (**Fig. 13**). The design shown in **Fig. 12a** was used to manufacture fatigue specimens with tangentially blending fillets. The stress ratio R = 0.1 and a frequency of f = 35 Hz were used for the cyclic fatigue testing. The failure criterion for the fatigue life was defined as the specimens' macroscopic failure. For the fatigue endurance limit, the 10^7 cycles run-out limit has been used and the fatigue behavior was studied in the high cycle region between 10^4 and 10^7 cycles.

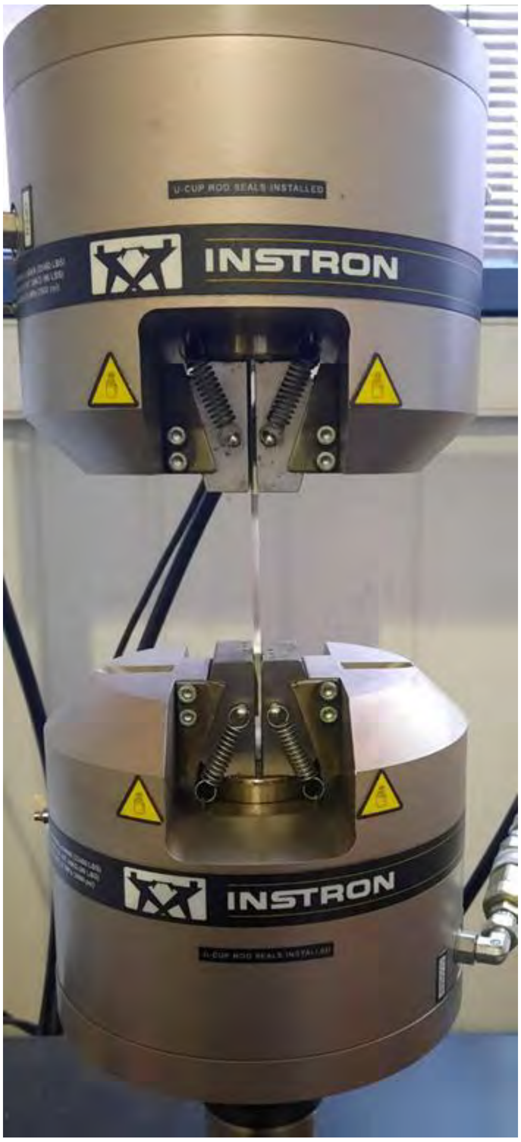

Fig. 13: Test configuration showing a dogbone-shaped fatigue specimen attached to the grips of the servo-hydraulic Instron 100 kN testing device

4.2.2 Fatigue crack growth (FCG) tests

Fatigue crack-growth testing was performed on the same apparatus with the constant amplitude fatigue tests, using C(T) type specimens with the geometry shown in **Fig. 12b**. The fatigue crack propagation experiments were carried out at a frequency of f = 15 Hz and a stress ratio of R = 0.1. An extensometer for measuring the crack opening displacement (COD) has been attached on the specimens' free surface at the side of the notch and the quantification of crack length was made on the basis of the compliance method (ASTM E647 [25]). Crack length measurements were verified also by direct observation using an optical system with a digital single-lens reflex (DSLR) camera and a macro lens (**Fig. 14**).

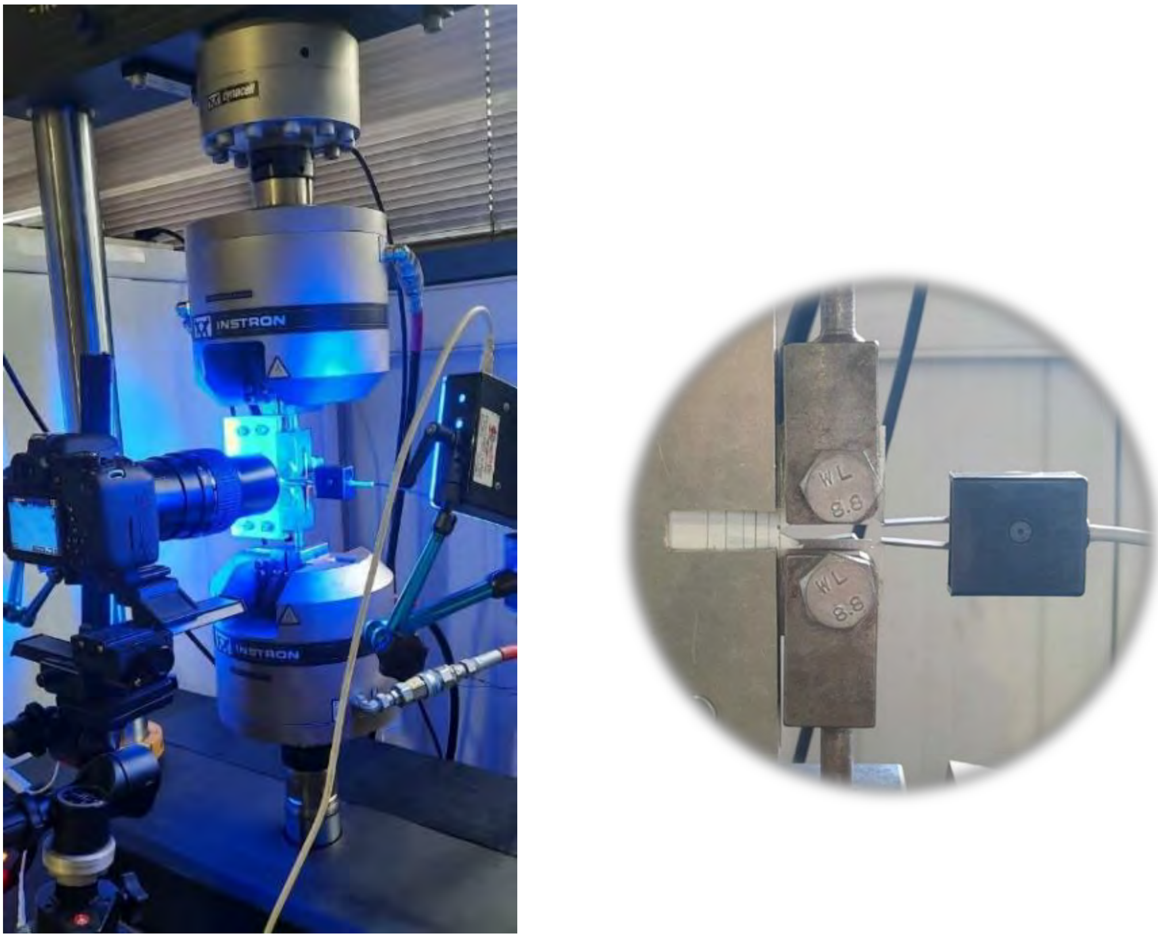

Fig. 14: COD gauge position attachment, anti-buckling apparatus and the digital single-lens reflex (DSLR) camera during fatigue crack growth (FCG) testing.

The initial pre-cracking stage was set at a crack length of 3.0 mm from the machined notch. The applied stress intensity factor range was defined based on compliance with the Linear Elastic Fracture Mechanics (LEFM) conditions set by the requirement:

$$\boldsymbol{W} - \mathbf{a} \geq \frac{4}{\pi}\left(\frac{K_{\max}}{\sigma_{\mathrm{y,0.2\%}}}\right)^2 \qquad (5)$$

where *W* is the specimen’s width equal to 48 mm in the present case, $\sigma_{y,0.2\%}$ is the conventional yield stress at 0.2 % axial strain value of the material, (*W* − a) refers to the uncracked ligament of the specimen and K_{max} corresponds to the maximum value of stress intensity factor for each crack length value. The maximum crack length to satisfy the LEFM requirement was found between 31 mm and 34 mm depending on the material.

For the C(T) specimen geometry, the stress-intensity factor range was calculated using the following formula:

$$\Delta K = \frac{\Delta P}{B\sqrt{W}} \frac{(2+a)}{(1-a)^{3/2}} (0.886 + 4.64a - 13.32a^2 + 14.72a^3 - 5.6a^4) \quad (6)$$

where α = a / W is the crack length to width ratio, B is the thickness of the specimen and ΔP is the applied load range.

Crack growth rates were evaluated on the basis of the Paris-Erdogan crack growth equation:

$$\frac{da}{dN} = C(\Delta K)^m \quad (7)$$

where m is equal to slope and C is the intercept crack growth rate for ΔK =1 MPa$\sqrt{m}$. The Paris-Erdogan coefficients were found by fitting the experimental da/dN-ΔK data to the ΔK band, which spans from 17 to 30 MPa√m, using the least squares approach.

Chapter 5: Results and discussion

5.1 Tensile behavior of AA2198

The tensile tests carried out at the Laboratory of Strength of materials, School of Applied Mathematical and Physical Sciences, National Technical University of Athens by Alexopoulos et al.[26]. **Fig. 15** depicts the tensile behavior of AA2198 at various artificial aging durations at 170°C. The precipitation of intermetallic phases and microstructure changes that occur with increased ageing time are linked to variations in tensile behavior.

The axial nominal strain, for example, continuously decreased with increasing ageing time up to 48 hours exposure to artificial ageing at 170 °C. This suggests that the 48 hours artificial ageing corresponds to the PA region for AA2198 at 170 °C. The specimens' axial nominal yield stress, on the other hand, increased with increasing ageing time and reached its maximum value after 48 hours at 170 °C. A small recovery of the axial nominal strain was seen, however nominal yield stress declined with further ageing times beyond 48 hours. At 400 hours of artificial aging, however, the axial nominal strain decreases further. Young modulus elasticity *E*, ultimate tensile strength σ_{uts}, conventional 0.2% yield stress $\sigma_{y,0.2\%}$ and uniform elongation ε_u are summarized in **Table 4** for all tempers.

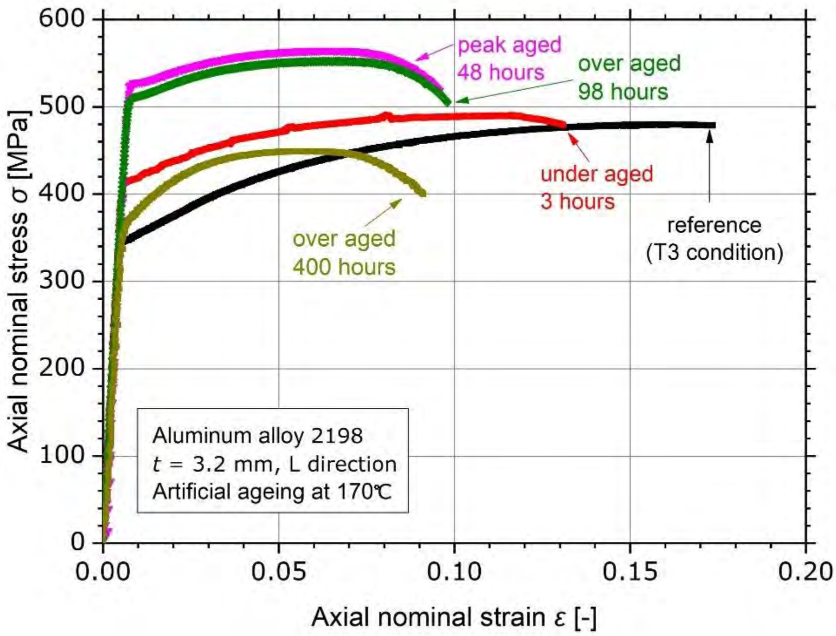

Fig. 15: Tensile test results of AA2198 exposed for different times to artificial ageing heat-treatment at 170° C[26]

Table 4: Tensile mechanical properties of the investigated artificial ageing conditions of AA2198.[26]

state	E	σ_{uts}	$\sigma_{y,0.2\%}$	ε_u
	(GPa)	(MPa)	(MPa)	(%)
T3 reference	71.6	482.5	349.2	15.8
Under aged	77.9	488.1	410.8	10.3
Peak aged	79.8	560.5	523.8	8.9
Over aged (98h)	72.5	496.2	511.7	6.4
Over aged (400h)	71.5	447.7	371.9	8.6

5.2 Constant amplitude fatigue behavior

In **Fig. 16** the fatigue S-N curves for the AA alloys with varying aging temperatures are displayed. In the diagrams, the maximum fatigue stress is plotted against the number of cycles required for failure on a semi-logarithmic scale. Run-out tests are indicated by the addition of a small arrow at the location of the data point. Artificial aging, irrespective of aging duration has a negative impact on fatigue performance in relation to the reference T3 state.

Based on the available experimental results, the fatigue endurance limit for 10^7 cycles is projected to be around 190 MPa for the T3 and under-aged treatment and 197 MPa for the peak-aged and over-aged tempers. This equates to a 3.5% increase in comparison to the respective fatigue limit. A 50% increase in tensile yield stress (≈ 524 MPa) between the peak-aged specimens and the reference material in T3 temper (≈ 349 MPa) does not translate into the expected improvement in fatigue behavior. This implies that although strength plays a major role in determining high cycle fatigue, strength by itself is not a trustworthy predictor of a material's anticipated fatigue performance.

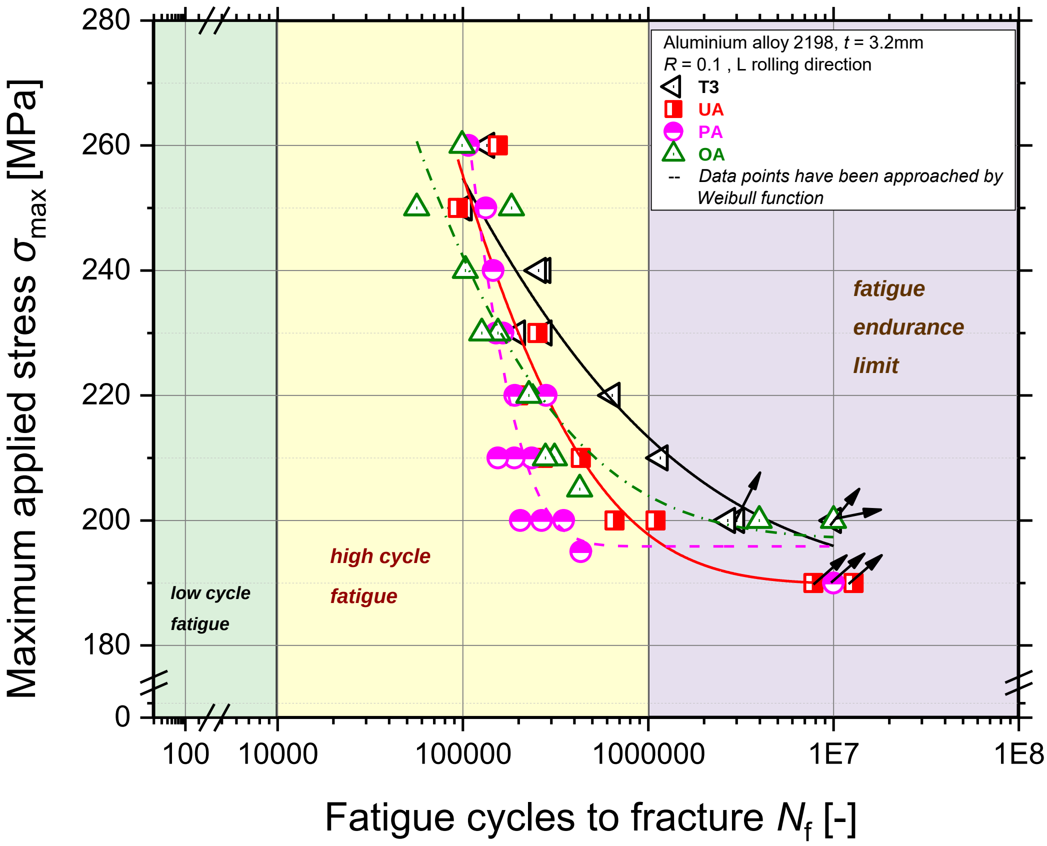

Fig. 16: Maximum applied stress – fatigue cycles to fracture curves derived from the constant amplitude fatigue tests for the different artificial ageing conditions of AA2198-T3.

The constant amplitude fatigue results were approximated using a four (4) parameter Weibull distribution by implementing the following equation:

$$\sigma_{max} = P_1 + \frac{P_2 - P_1}{\exp\left(\frac{\log N_f}{P_3}\right)^{P_4}} \qquad (8)$$

The average σ_{uts} value for each material, as established by the corresponding tensile tests, has been utilized for the parameter P_2. Using Eq. 6, the coefficients P_1, P_3, and P_4 from the Weibull fitting analysis were determined. Parameter P_1 in the performed analysis approximates the fatigue endurance limit [27]**Σφάλμα! Το αρχείο προέλευσης της αναφοράς δεν βρέθηκε.**. **Table 5** summarizes the calculated Weibull coefficients for the different investigated artificial ageing conditions of AA2198.

Table 5: Weibull coefficients (average values and standard deviation) of the investigated constant amplitude fatigue

Condition	P_1 [MPa]	P_2 [MPa]	P_3 [MPa]	P_4 [MPa]
T3	190.19 ± 13.28	482	4.32 ± 0.13	2.84 ± 0.88
UA	189.79 ± 7.58	488	4.58 ± 0.17	4.77 ± 1.42
PA	195.85 ± 6.28	560	4.79 ± 0.08	10.92 ± 2.92
OA	196.91 ± 9.50	554	4.07 ± 0.27	3.53 ± 1.22

For the mathematical representation of the S-N curves, a Basquin-type analysis has been carried out for the quantitative evaluation of the fatigue results. The Basquin equation has been used in the form of:

$$\boldsymbol{\sigma}_{\mathbf{a,eq}} = \boldsymbol{\sigma}_{\mathbf{f}'}\ (\mathbf{2}\boldsymbol{N}_{\mathbf{f}})^{\boldsymbol{b}} \qquad \textbf{(9)}$$

where b is the slope of the curve in log-log scale and constant $\sigma_{f'}$ is the intercept at N_f = 0.5 cycles. The coefficients b and $\sigma_{f'}$ have been determined using a least square fitting method in the high cycle fatigue region (10^4-10^6 fatigue cycles) on a log-log scale plot.

For the Basquin-type approximation, the equivalent stress amplitude for zero mean stress $\sigma_{a,eq}$ has been estimated using the Goodman mean stress correction equation with the expression:

$$\boldsymbol{\sigma}_{\mathbf{a,eq}} = \frac{\boldsymbol{\sigma}_{\mathbf{a}}}{\mathbf{1}-\frac{\boldsymbol{\sigma}_{\mathbf{m}}}{\boldsymbol{\sigma}_{\mathbf{uts}}}} \qquad \textbf{(10)}$$

where σ_{a} is the stress amplitude for stress ratio R = 0.1, σ_{m} is the mean stress and σ_{uts} the ultimate tensile strength of the material.

The fatigue curve of T3 material was characterized by the smallest b exponent corresponding to the slope of the S-N curve. A small b value shows a smooth transition of fatigue lives with variation from higher to lower stresses approaching the fatigue limit. The exponent b values in the under- and over-aged conditions have similar values, while the highest b value was obtained in the peak-aged condition which is reflected in a steep S-N curve behavior (**Table 6** and **Fig. 16**).

Table 6: Basquin equation coefficients of the different investigated ageing conditions of AA2198.

Condition	*b* [-]	$\sigma_{f'}$ [MPa]
T3	-0.10289	561
UA	- 0.14436	908
PA	-0.24202	2847
OA	-0.14901	893

The S-N curves of AA2198 in various ageing tempers are shown in **Fig. 17**, taking into consideration the normalized maximum stress over the $\sigma_{y,0.2\%}$ and σ_{uts} values (**Fig. 17a** and **b** respectively). Viewed from this angle, the T3 material exhibits fatigue behavior in a larger stress range than the other tempers, making the variations in its fatigue performance clearer, that corresponds to roughly 60–75% and 42–54% of the conventional 0.2% yield stress and ultimate tensile strength, respectively. In the UA condition, the fatigue behavior exists in the range of 45 to 60 % with regard to the material's $\sigma_{y,0.2\%}$ and 38 to 53 % with respect to σ_{uts}, while for the PA material the behavior is exhausted at 37 to 50 % of the $\sigma_{y,0.2\%}$ and 34 to 46 % of the σ_{uts} values.

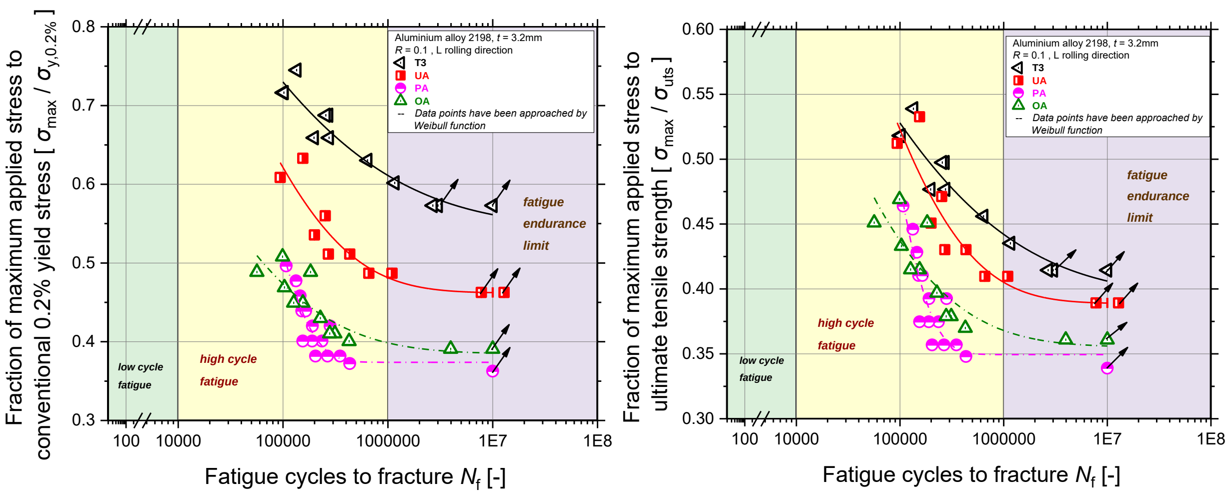

(a) **(b)**

Fig. 17: Normalized stress – fatigue life curves in function with (a) conventional 0.2 % yield stress and (b) ultimate tensile strength of constant amplitude fatigue tests of AA2198 for the different investigated artificial ageing conditions.

5.3 Fatigue crack growth rate

In Fig. 18, the crack advancement versus number of cycles for the reference T3 material as well as for the artificial aged alloys is shown. In comparison to the materials in under-, peak-, and over-aged state, the AA2198 in T3 condition exhibits a superior damage tolerance behavior in terms of damage tolerance capacities. The diagram displays the fatigue crack growth behavior in the region extending from the initial pre-cracking length (3mm) to the final crack length satisfying the linear elastic fracture mechanics theory. As indicated in **Table 7**, the T3 material displays the highest number of fatigue cycles in the specific range, albeit showing a slightly increased experimental fatigue life' scatter when compared to the other tempers. The fatigue lifetimes of AA2198 are comparable for all four (4) tempers with the OA for 400 hours to show, slightly, the lowest number of fatigue cycles. In addition, the T3 temper exhibits a delayed crack initiation phase indicating a 60% increase in the number of cycles to reach the notch pre-cracking length of 3 mm, with regard to the other alloys.

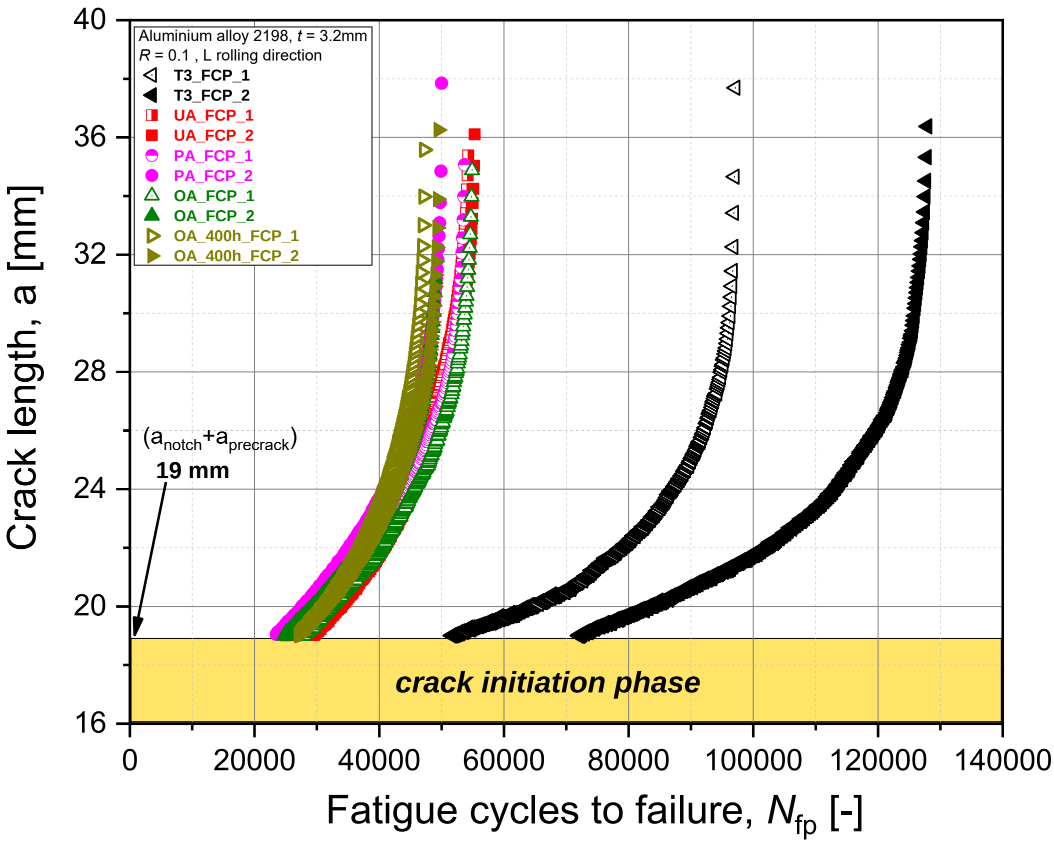

Fig. 18: Crack length versus fatigue cycles to failure curves for fatigue crack propagation tests.

Table 7: Number of fatigue cycles to failure and Paris-Erdogan equation coefficients of the different aging tempers for fatigue crack propagation tests.

Code name	Fatigue cycles to failure N_f	Average cycles to failure value	Standard Deviation	*m* [-]	$C\left(\frac{mm/cycle}{(MPa\sqrt{m})^m}\right)$
T3_FCP_1	97,100	112,500	21,778	4.238	9.64E-10
T3_FCP_2	127,900			4.040	1.30E-09
UA_FCP_1	54,300	54,800	707	2.336	3.98E-07
UA_FCP_2	55,300			2.281	5.35E-07
PA_FCP_1	53,700	51,850	2616	2.923	7.38E-08
PA_FCP_2	50,000			3.025	5.22E-08
OA_FCP_1	54,900	51,950	4171	3.390	1.66E-08
OA_FCP_2	49,000			4.165	1.87E-09
OA_400h_FCP_1	47,200	48,350	1626	3.095	5.96E-08
OA_400h_FCP_2	49,500			3.470	1.70E-08

By observing the fatigue crack growth rate data in terms of the da/dN – ΔK curves of **Fig. 19**, it is possible to verify the superior crack growth behavior emanating from the notch. In comparison to the UA, PA, OA(98h) and OA(400h) conditions, the average crack development rates for the T3 state are 49%, 51%, 51% and 48% lower for low ΔK values, which range from 15 to 20 MPa√m. However, the capacity of the T3 material to withstand fatigue cracking seems to deteriorate more appreciably with the increase of the applied ΔK values in regard to other tempers. The T3 crack growth rates tend to converge with the rates of the UA and PA condition at medium (25 MPa√m) and high (30 MPa√m) ΔK, respectively, as shown in the graphs of **Fig. 19(a)-(c)**. Additionally, across the whole ΔK range under investigation, the FCP rates of both OA conditions remain higher than the T3 state.

Fig. 19(d) compares the da/dN - ΔK curves of the three investigated artificial aging conditions. The artificial aging of the material does not appreciably change the crack growth rate at low ΔK values (15 to 20 MPa√m). Crack growth rates are lower in the UA material above 25 MPa√m than in the PA and OA situations. It is important to note that the OA condition has the highest rate of crack propagation, especially for ΔK values greater than 25 MPa√m and for 400 hours artificial aging time.

The fatigue crack growth equation constants obtained empirically and shown in **Table 7** are consistent with the material trends discussed above. The T3 state has the lowest C value in the group, despite the fact that its exponent m is the largest for this particular material. Crack propagation rates in the OA condition are higher than other materials at lower ΔK levels and comparable to the T3 state for ΔK values larger than 25 MPa√m. This fact makes the OA(98h) temper the less-damage tolerant material, exhibiting the highest crack propagation rates in the range of 15 to 30 MPa√m. In comparison to other materials, it exhibits a low *C* value (9.25 x 10^{-09} on average) and a high *m* (3.78 on average), which together characterize its behavior. The variation in the empirical parameters *C* and *m* with increasing aging time is seen in **Fig. 20**. The T3 temper is used as a point of reference, and with the exception of the UA, it is shown that while the *m* value rises with prolonged exposure to aging treatment, the *C* value decreases with increased ageing time. In the case of OA(400h) temper the *m* value appears a decrease and *C* value a slightly increase. In this case the combined high values of constants C, m are responsible for the high values of crack growth rates. When the T3 state and the UA condition are compared, a sharp decrease and rise in the *m* and *C* values of the UA, respectively, are observed.

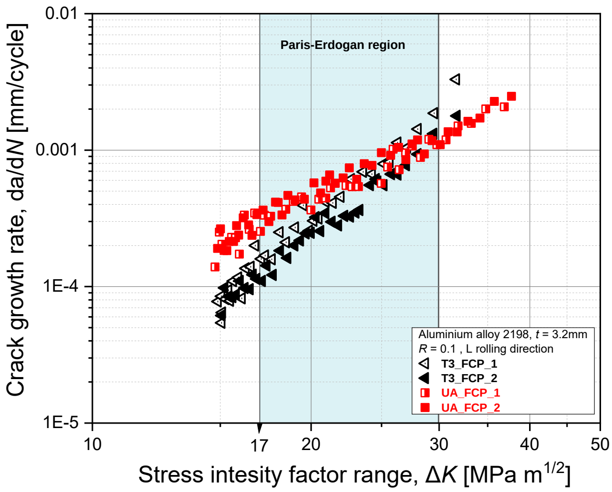

(a)

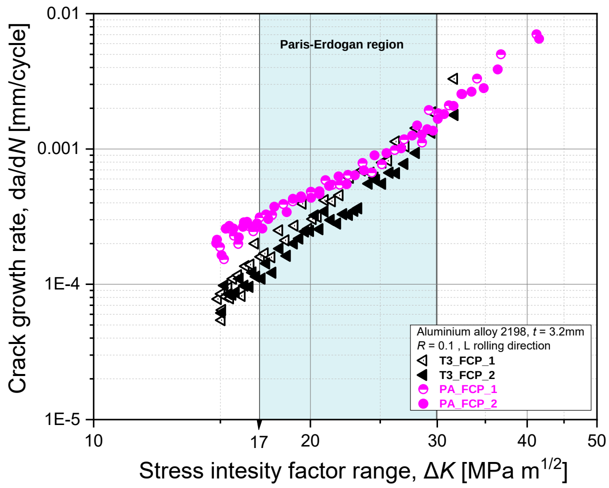

(b)

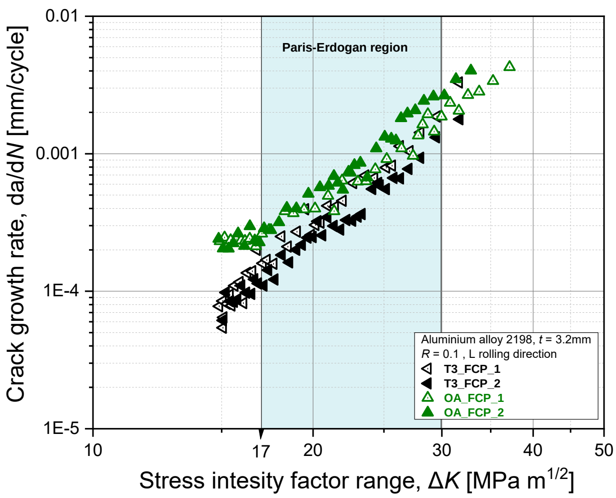

(c)

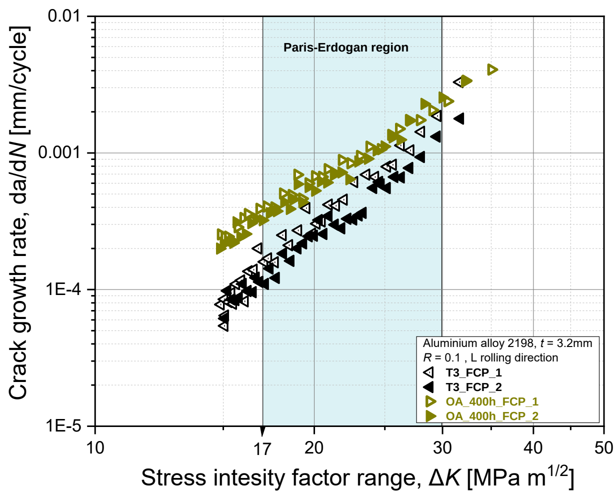

(d)

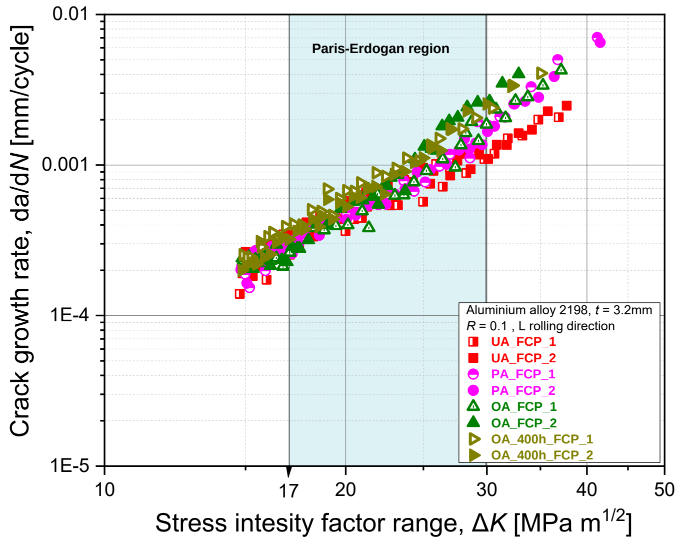

(e)

Fig. 19: Crack propagation rate da/dN versus ΔK diagrams: comparison between AA2198-T3 with the investigated (a) under-aged, (b) peak-aged, (c) over-aged (98 hours), (c) over-aged (400 hours) conditions. Diagram (e) shows the comparison of all the artificial aged conditions.

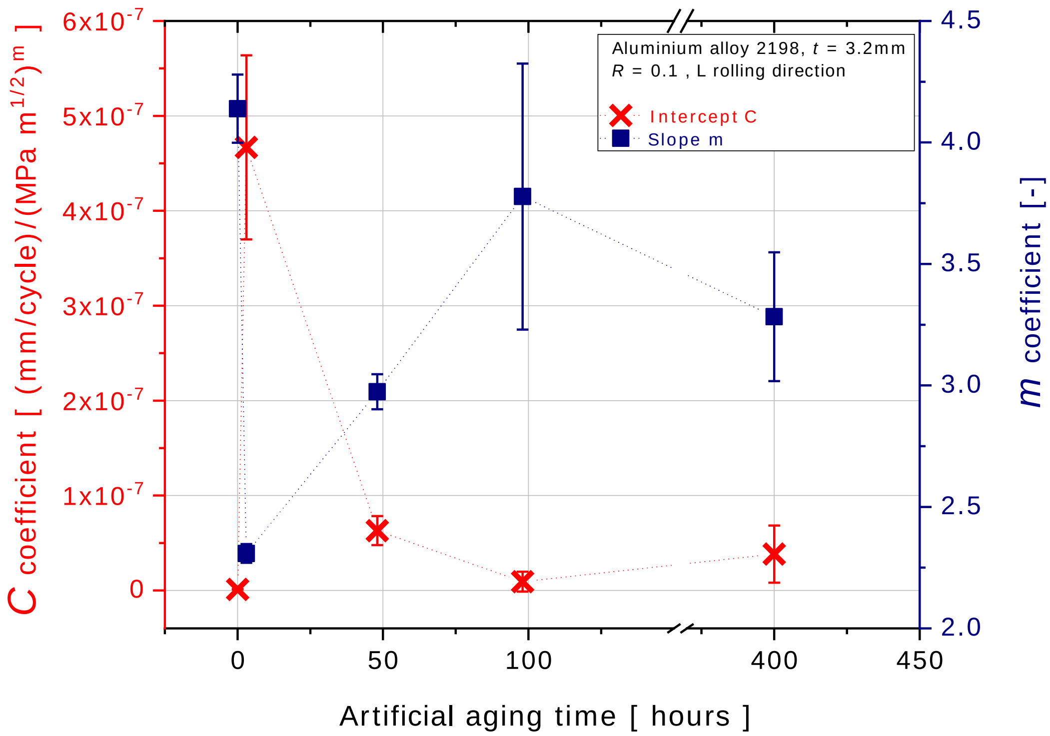

Fig. 20: Paris-Erdogan coefficients versus ageing time in double-y axis.

Chapter 6: Summary and conclusions

The present master thesis contributes to the knowledge on the mechanical behavior of aeronautical aluminum alloy AA2198 by providing new, valuable information on their mechanical properties under cyclic loading and by focusing on the experimental investigation of the effect of artificial aging on the constant amplitude fatigue and fatigue crack growth behavior. The main findings resulting from the experimental investigation are:

- The AA2198-T3 shows generally improved high cycle fatigue behavior when compared to aged alloys. This is confirmed with the small *b* exponent on the fatigue curve of T3 material indicates a smooth transition from higher to lower stresses as it approaches the fatigue limit.
- Experimental data indicates a 3.5% increase in 10^7 cycles fatigue endurance limit, from T3 and UA conditions to PA and OA tempers.
- Peak-aged specimens with 50% higher tensile yield stress do not improve fatigue behavior, suggesting that strength alone cannot reliably reflect a material's expected fatigue, despite high cycle fatigue being a strength-driven property.
- AA2198 exhibits superior damage tolerance in T3 condition. The T3 material's fatigue cracking resistance capacity deteriorates with increasing applied ΔK values, with T3 crack growth rates convergent with UA and PA conditions at medium and high ΔK, while OA conditions have higher rates.
- The T3 material's fatigue cracking capacity deteriorates with increasing applied ΔK values, with T3 crack growth rates convergent with UA and PA conditions at medium and high ΔK, while OA conditions have higher rates.
- The T3 material has the highest exponent m but the lowest C value. In the OA condition, crack propagation rates are similar to T3 state, making it less damage-tolerant. Its behavior is described by high m and low C value.

6.1 Recommendation for future research

- Study of corrosion effect on artificial aged AA2198 both on constant amplitude fatigue behavior and fatigue crack growth.
- Crack closure measurements to better describe the fatigue crack growth behavior.
- Carrying out the experiments with a higher stress ratio i.e. R=0.5

References

[1] R. J. Rioja and J. Liu, “The evolution of Al-Li base products for aerospace and space applications,” *Metall Mater Trans A Phys Metall Mater Sci*, vol. 43, no. 9, 2012, doi: 10.1007/s11661-012-1155-z.

[2] N. D. Alexopoulos, E. Migklis, A. Stylianos, and D. P. Myriounis, “Fatigue behavior of the aeronautical Al-Li (2198) aluminum alloy under constant amplitude loading,” *Int J Fatigue*, vol. 56, 2013, doi: 10.1016/j.ijfatigue.2013.07.009.

[3] Y. Lin, C. Lu, C. Wei, and Z. Zheng, “Effect of aging treatment on microstructures, tensile properties and intergranular corrosion behavior of Al–Cu–Li alloy,” *Mater Charact*, vol. 141, 2018, doi: 10.1016/j.matchar.2018.04.043.

[4] H. Li, Y. Tang, Z. Zeng, Z. Zheng, and F. Zheng, “Effect of ageing time on strength and microstructures of an Al-Cu-Li-Zn-Mg-Mn-Zr alloy,” *Materials Science and Engineering: A*, vol. 498, no. 1–2, 2008, doi: 10.1016/j.msea.2008.08.001.

[5] Y. Zhang, J. Ling, H. G. Li, X. Y. Luo, and Z. X. Ba, “Effect of pre-deformation and artificial aging on fatigue life of 2198 Al-Li alloy,” *Mater Res Express*, vol. 7, no. 4, Apr. 2020, doi: 10.1088/2053-1591/ab83a6.

[6] P. S. Pao, L. A. Cooley, M. A. Imam, and G. R. Yoder, “FATIGUE-CRACK GROWTH IN 2090 Al-Li ALLOY,” 1989.

[7] R. Sepe, V. Giannella, N. Razavi, and F. Berto, “Characterization of static, fatigue and fracture behaviour of the aluminium-lithium alloy Al-Li 2198-T851,” *Int J Fatigue*, vol. 166, 2023, doi: 10.1016/j.ijfatigue.2022.107265.

[8] Z. jie MENG *et al.*, “Low cycle fatigue behavior and fatigue life prediction of 2195 Al-Li alloy at warm temperatures,” *Transactions of Nonferrous Metals Society of China (English Edition)*, vol. 33, no. 9, pp. 2574–2587, Sep. 2023, doi: 10.1016/S1003-6326(23)66282-X.

[9] Y. Chen, X. Pan, C. Zhang, Z. Cui, and C. Ji, “Influence of foreign object impact mode on fatigue performance of 2198-T8 Al-Li alloy thin sheets for fuselage,” *Fatigue Fract Eng Mater Struct*, vol. 44, no. 1, 2021, doi: 10.1111/ffe.13338.

[10] Goran Djukanovic, “Aluminium-Lithium Alloys Fight https://aluminiuminsider.com/aluminium-lithium-alloys-fight-back/.”

[11] “https://en.wikipedia.org/wiki/Comac_C919.”

[12] "Mavis Toh, C919 advances with mid-fuselage completion, https://www.flightglobal.com/c919-advances-with-mid-fuselage-completion/114308.article [28 August 2014]."

[13] A. Hiken, "The Evolution of the Composite Fuselage - A Manufacturing Perspective," *SAE International Journal of Aerospace*, vol. 10, no. 2, pp. 77–91, Sep. 2017, doi: 10.4271/2017-01-2154.

[14] "Spacex [ONLINE], Available:https://web.archive.org/web/20101222155322/http://www.spacex.com/falcon9.php."

[15] "https://en.wikipedia.org/wiki/Space_Shuttle_external_tank."

[16] K. I. T. Σπύρος Γ. Παντελάκης, *Μηχανική Συμπεριφορά Υλικών "Καμπύλες τάσης-Διάρκειας ζωής."* Thessaloniki, 2018.

[17] K. I. T. Σπύρος Γ. Παντελάκης, *Μηχανική Συμπεριφορά Υλικών "Διάδοση ρωγμών λόγω κόπωσης."* Thessaloniki, 2018.

[18] Norman E. Dowling, "Mechanical Behavior of Materials," 2013.

[19] G.N.Haidemenopoulos, S.G.Pantelakis, and J.R.Kissell, "Handbook of advanced Materials, 'Aluminum and aluminum alloys,'" 2004, pp. 321–327.

[20] J. S. Jesus *et al.*, "Influence of specimen orientation on fatigue crack growth in 7050-T7451 and 2050-T8 aluminium alloys," *Int J Fatigue*, vol. 164, 2022, doi: 10.1016/j.ijfatigue.2022.107136.

[21] *Γρηγόρης Ν.Χαϊδεμενόπουλος, Ισχυροποίηση με Καθίζηση, Φυσική Μεταλλουργία, Εκδόσεις Τζιόλα, Θεσσαλονίκη, 499-502, 2018*.

[22] "N.D. Alexopoulos, A. Proiou, T.N. Examilioti, N. Kashaev, S. Riekehr, S.K. Kourkoulis, Mechanical performance of (Al-Cu) 2024 and (Al-Cu-Li) 2198 aluminum alloys under different artificial ageing conditions, Procedia Structural Integrity 2 (2016) 3782-3783.".

[23] *L. F. Mondolfo, Aluminum Alloys – Structure and Properties, Butterworth, London, 1976.*

[24] ASTM E466, "Standard Practice for Conducting Force Controlled Constant Amplitude Axial Fatigue Tests of Metallic Materials 1," West Conshohocken, Jun. 2002.

[25] ASTM E647, "Standard Test Method for Measurement of Fatigue Crack Growth Rates 1," West Conshohocken, Apr. 2001.

[26] T. N. Examilioti *et al.*, “On anisotropic tensile mechanical behavior of Al–Cu–Li AA2198 alloy under different ageing conditions,” *Journal of Materials Research and Technology*, vol. 24, pp. 895–908, May 2023, doi: 10.1016/j.jmrt.2023.02.206.

[27] S. G. Pantelakis, A. N. Chamos, and A. T. Kermanidis, “A critical consideration for the use of Al-cladding for protecting aircraft aluminum alloy 2024 against corrosion,” *Theoretical and Applied Fracture Mechanics*, vol. 57, no. 1, pp. 36–42, Feb. 2012, doi: 10.1016/j.tafmec.2011.12.006.